Journal of Applied Pharmaceutical Science Vol. 8(08), pp 129-137, August, 2018
Available online at http://www.japsonline.com
DOI: 10.7324/JAPS.2018.8818
ISSN 2231-3354

Enhanced Electrocatalytic Activity of Pd–Ir–Ni, Pd–Ir–Mo and Pd–Ir–Rh Nanoparticles Supported on Cellulose-based Carbon (CC) for Membraneless Sodium Perborate Fuel Cells (MLSPBFCs)

K. Vijayaramalingam[1], A. Karthikeyan[1], V. Selvarani[1], S. Kiruthika[2], B. Muthukumaran[1*]

[1]Department of Chemistry, Presidency College, Chennai 600 005, India.
[2]Department of Chemical Engineering, SRM University, Chennai 603 203, India.

ARTICLE INFO

Article history:
Received on: 30/03/2018
Accepted on: 25/05/2018
Available online: 31/08/2018

Key words:
Sodium perborate, Fuel cell, Hydrogen peroxide, Cellulose based carbon, trimetallic catalyst, Pd–Ir–M.

ABSTRACT

In the present study, a new concept of fabrication, characterization, and performance of Pd–Ir–M ternary nanoparticles supported on cellulose-based carbon (CC) was proposed with a notion to enhance the electrocatalytic oxidation of hydrogen peroxide. The combination of monometallic Pd/CC, bimetallic Pd–Ir/CC, and tri-metallic Pd–Ir–M/CC (M = Ni, Mo, and Rh) nanoparticles were synthesized by the chemical reduction method assisted by ultrasonication. X-Ray diffraction (XRD), energy dispersive X-Ray spectroscopy (EDX), transmission electron microscopy (TEM) and scanning electron microscopy (SEM) were used for the catalyst characterization. The catalytic activities of electrocatalysts were measured in half-cell experiments using chronoamperometry (CA), CO stripping voltammetry, and cyclic voltammetry (CV). Based on half-cell experiments, electrochemical results showed that tri-metallic Pd–Ir–M nanoparticles display better catalytic activity at room temperature towards hydrogen peroxide oxidation as compared to bimetallic and monometallic catalysts. Based on the experiments carried out on MLSPBFC, Pd–Ir–Ni/CC displayed a better catalytic activity than all other catalysts synthesized.

INTRODUCTION

In recent years, metal nanoparticles supported on cellulose-based carbon (CC) nanoparticles have earned special consideration as they are highly promising catalyst substances for fuel cells, electronic sensor devices, and hydrogen storage because of their electrochemical, electromagnetic, and structural characteristics (Georgakilas *et al*., 2007; Correa-Duarte and Liz-Marzan, 2006). However, because of the huge cost of transition metals for the catalyst (specifically Pd), the loading should be reduced to a level of < 2.0 mg cm^{-2} (Liu *et al*., 2006). Although the nanoparticle-type approach could really minimize Pd content in the electrocatalysts, CO poisoning effect where the active sites are badly screened can suppress the reaction kinetics and shorten the lifetime of fuel cells (Jin and Chen, 2007). By employing binary, ternary, and quaternary alloy nanoparticles, CO poisoning problem can be overcome (Ryu *et al*., 2010; Jin and Chen, 2007; Liu *et al*., 2006; Lamy *et al*., 2002). However, the adsorption of metal alloy nanoparticles over cellulose based carbons uniformly is also very difficult, and typical impregnation approaches suffer from disadvantages like tedious process and contamination of catalysts by the formation of side products (Zhang *et al*., 2008; Che *et al*., 1999; Grag and Sinnott, 1998). More particularly, the preparation of binary and ternary metal nanoparticles is highly troublesome when compared with pure ones due to the drawbacks in the homogeneous formation of alloy and controlling the distribution of metals.

The MLSPBFCs have attracted notable consideration for utilization in compact electronics, residential power sources, and shipment because of the higher energy density, comparably low operating temperatures, zero or lesser discharge of toxic wastes, and minimum decomposition issues. However, the commercial growth of MLSPBFCs is still inhibited by various components containing

*Corresponding Author
B. Muthukumaran, Assistant professor, PG research & department of Chemistry, Presidency College, Chennai 600 005, Tamil Nadu, India.
E-mail: dr.muthukumaran @ yahoo.com

inadequate electrocatalytic activity of electrodes both for hydrogen peroxide oxidation reaction (HPOR) and oxygen reduction reaction (ORR), huge cost of Pd-based catalysts, and sensitivity of the electrocatalysts to be affected by CO-like intermediates produced during HPOR (Bennett *et al*., 2012; Park *et al*., 2012; Umeda *et al*., 2012; Zhao *et al*., 2012; Zheng *et al*., 2012). The best solution to these drawbacks is to combine palladium with other metals such as Iridium (Ir), Nickel (Ni), Cobalt (Co), and so on (Shahrokhian and Rastgar, 2011; Zhao *et al*., 2007; Cui *et al*., 2006), and develop the morphology and distribution of metals on proper supports (Nethravathi *et al*., 2011; He *et al*., 2007; Rodriguez-Nieto *et al*., 2004). By the combination of active sites, promoters, and supports, the catalyst can be optimized. Binary & ternary catalysts are considered as an encouraging option due to the interaction between the metals. This will modify the properties of the catalysts and will result in the improvement of the catalytic activity (Ribeiro *et al*., 2017). In recent years, various Pd-based bimetallic catalysts have been studied (Escudero-Cid *et al*., 2012; Kakati *et al*., 2012; Kang *et al*., 2012). Among them, binary Pd–Ir mixture is a famous candidate as an MLSPBFC's anode, as it displays a high electrocatalytic activity for HPOR and strong resistance against carbon monoxide contamination (Ahn *et al*., 2012; Li *et al*., 2012; Basnayake *et al*., 2006). Ir in Pd–Ir alloy easily oxidizes CO intermediate to CO_2 by a bifunctional mechanism (Wei *et al*., 2006); but, the performance of binary Pd–Ir alloy catalyst in hydrogen peroxide oxidation still needs to be improved (Wang *et al*., 2008). In order to enhance the catalytic activity of the Pd–Ir alloy and reduce the cost, three major issues need to be considered concerning the addition of a third metal (Yang *et al*., 2012; Xiong *et al*., 2005), the morphology of the nanoparticles and the nature of support. As a new form of carbon, cellulose-based carbon (CC) nanoparticles have been regarded as a new support for metal catalysts because of their small size, high chemical, thermal, mechanical stabilities, and their large surface area to volume ratio (Prabhuram *et al*., 2006; Collins *et al*., 1997; Dillon *et al*., 1997). The addition of a third metal (Ni, Mo, Sn, Ce, and Rh, etc.) improves the performance of the Pd–Ir electrode (Guillen-Villafuerte *et al*., 2012; Huang *et al*., 2009; Jeon *et al*., 2008). Among them, despite the controversies, recent studies have shown that the addition of Ni, Mo, and Rh to Pd and Pd–Ir catalysts can enhance the electrocatalytic activity for hydrogen peroxide oxidation (Li *et al*., 2013; Tusi *et al*., 2013; Wang *et al*., 2011; Liu *et al*., 2006). The enhanced activity of the ternary catalyst is because of the promoting effect of the second or third elements added to palladium as shown in Table 1. In this study, a facile method, that is, a chemical reduction process assisted by ultrasonication was proposed to prepare well-dispersed Pd–Ir–Ni, Pd–Ir–Mo, and Pd–Ir–Rh catalysts supported on cellulose-based carbon (CC) nanoparticles was proposed, and the performance of an MLSPBFC with these catalysts as the anode catalysts for hydrogen peroxide electro-oxidation was investigated.

Table 1: Comparison of electrochemical activity of catalysts.

Catalyst	On-set voltage (V)	Current density (mA/cm²)
Pd/C	0.35	1.43
Pd–Ir/C	0.29	2.6
Pd–Ir–Ni/C	0.28	2.9
Pd–Ir–Ce/C	0.27	2.68

EXPERIMENTAL

Chemicals and materials

For catalysts preparation, the metal precursors used were palladium (II) nitrate dihydrate ($Pd(NO_3)_2.2H_2O$) (Merck), iridium (III) chloride hydrate ($IrCl_3.H_2O$) (Merck), nickel (II) chloride hexahydrate ($NiCl_2.6H_2O$) (Alfa Aesar), sodium molybdate dihydrate ($Na_2MoO_4.2H_2O$) (Alfa Aesar) and rhodium (III) chloride trihydrate ($RhCl_3.3H_2O$) (Merck). Microcrystalline cellulose powder (Arjun Chemicals) was utilized as a base for the electrocatalysts. Ethylene glycol (EG) (Merck) was taken both as the reducing agent and as the solvent. Nafion® dispersion (DE 521, DuPont USA) was used for catalyst ink preparation. For electrochemical analysis, sodium perborate (Riedel) was used both as a fuel and as an oxidant and H_2SO_4 (from Merck) was used as an electrolyte. All the materials used were of AR grade materials. For cathode catalyst, Pd/C (40-wt%, from E-TEK) was used.

Catalyst synthesis

Synthesis of cellulose-based carbon support

Cellulose-based carbon was prepared by mixing the microcrystalline cellulose with water and was kept at 5°C for 2 hours in order to allow the swelling of fibre. Caustic solution was cooled, and cellulose was added to it. Mixing was performed under the cooling condition for 2 hours with a stirring rate of 1000 rpm. The solution was then poured into a mould and then heated for 20 hours at 50°C. The cellulose was then washed with water to remove excess of sodium hydroxide, till the pH becomes neutral (7.0). After washings, the material was dried under supercritical conditions (Gavillon and Budtova, 2008).

Synthesis of nanoparticles

The binary (Pd–Ir/CC) and ternary (Pd–Ir–Ni/CC, Pd–Ir–Mo/CC and Pd–Ir–Rh/CC) nanoparticles were synthesized by the chemical reduction process assisted by ultrasonication. The Pd–Ir, Pd–Ir–Ni, Pd–Ir–Mo and Pd–Ir–Rh content was 40 wt.% in each sample and the atomic ratios of Pd:Ir and Pd:Ir:M (M = Ni, Mo and Rh) were 1:1 and 6:3:1 respectively. Initially, 2.67 mL of $Pd(NO_3)_2$ (0.038 M) in EG and 2.78 mL of $IrCl_3$ (0.036 M) in EG were mixed with EG (50 mL) in a multi-necked flask. To the prepared EG solution, 70 mg of CC was added, and the pH was increased to 9.0 using NaOH (0.5 M) in EG. The mixture had been ultrasonicated for 30 minutes, kept in a microwave oven and then heated for 3 minutes. The mixture was filtered and then the filtered catalyst was washed with ethanol followed by deionized water. The filtration process was carried out multiple times. In the end, the Pd–Ir/CC catalyst was dried under vacuum for 5 hours at 80°C. The synthesis of Pd–Ir–M/CC (M = Ni, Mo and Rh) electrocatalysts was identical to that of the Pd–Ir/CC electrocatalyst, except that the relevant quantity of $Pd(NO_3)_2$, $IrCl_3$, $NiCl_2$, Na_2MoO_4 and $RhCl_3$ in EG were mixed in the solution.

Structural catalyst characterization

The size of the distributed electrocatalysts had been investigated by TEM (Philips CM 12 Transmission Electron Microscope) and SEM (ZEISS EVO 50 Scanning Electron

Microscope). TEM was also used to calculate the particle size dispersion and average particle size. Powder X-Ray diffraction (XRD) technique was used to identify the crystal structure of the prepared catalysts by using a Rigaku multiflex diffractometer (model RU-200 B) with a Cu-$K_{\alpha 1}$ radiation source ($\lambda_{K\alpha 1}$ = 1.5406 Å) with the tube current of 40 mA and the tube voltage of 40 kV, performed at room temperature. The $2\theta^{\theta}$ angular area in the range of 20º and 90º was reported at 5° min^{-1} scan rate. The average particle morphology interpreted from TEM was checked by using Scherrer formula to determine the size of crystallite from the XRD pattern (Radmilovic *et al*., 1995). To measure the size of crystallite, the Pd (2 2 0) diffraction peak was chosen and by using the Bragg's equation, the lattice parameters of palladium alloy nanoparticles were obtained. An EDX analyzer associated with TEM was used to determine the metallic composition of the catalysts.

Electrochemical calculations and preparation of electrode

All electrochemical calculations were performed by an electrochemical workstation (CHI-6650; CH Instruments, USA) in a regular three-electrode cell assembly containing a glassy carbon disk, a Pd foil, and Ag/AgCl as a working electrode, as a counter electrode and as a reference electrode respectively. The preparation of glassy carbon electrode was done by taking 10 mg of Pd/CC, Pd–Ir/CC, Pd–Ir–Ni/CC, Pd–Ir–Mo/CC and Pd–Ir–Rh/CC electrocatalysts initially and were immersed separately in a solvent mixture (isopropyl alcohol (0.5 mL), DI water (0.5 mL) and 5 wt.% Nafion solution (0.1 mL, DuPont) and ultrasonicated for 20 minutes. Ultrasonically homogenized ink (0.01 mL) was drop-coated on a freshly refined glassy-carbon electrode (A = 0.125 cm^2) and the slurry was then kept at room temperature to evaporate the solvent in open air. The metal loading on the working electrode was 0.28 mg_{metal} cm^{-2}. The electrochemically active surface areas (ECASA) of the Pd/CC, Pd–Ir/CC, Pd–Ir–Ni/CC, Pd–Ir–Mo/CC and Pd–Ir–Rh/CC electrocatalysts were found out using CO stripping voltammetry in 0.5 M H_2SO_4 solution. Adsorption of CO on the electrode surface was obtained at 100 mV vs. Ag/AgCl in a CO-saturated solution for 10 minutes and flushed with nitrogen for 10 minutes for purification of the electrolyte by evacuating the CO adsorption on the sides. By using 0.15 M hydrogen peroxide and 0.5 M H_2SO_4 solutions, the electrochemical activity of the HPOR was calculated by CV in a half cell with a scan rate of 50 mV s^{-1} at room temperature. In this study, all potentials were measured vs. Ag/AgCl.

RESULTS AND DISCUSSION

Physical characterization

X-ray diffraction (XRD)

X-Ray Diffraction (XRD) analyses were conducted to obtain the structural data of electrocatalysts. Figure 1 shows the XRD patterns of Pd/CC, Pd–Ir/CC, Pd–Ir–Rh/CC, Pd–Ir–Mo/CC, and Pd–Ir–Ni/CC nanoparticles in which distinctive peaks of CC are observed (2θ = 25.6°). The diffraction peaks at approximately 39.6°, 46.7°, 67.8°, and 81.8° were associated with Pd (1 1 1), (2 0 0), (2 2 0) and (3 1 1) crystalline planes, respectively, defining a regular aspect of the crystalline Pd with an "fcc" (face-centred cubic) structure. However, when compared with reflections of pure Pd/CC, diffraction peaks of Pd–Ir/CC and Pd–Ir–M/CC (M = Ni, Mo and Rh) nanoparticles moved a little to bigger 2θ values. The marginal shifts of diffraction peaks displayed the alloy formation including incorporation of Ir and M (M = Ni, Mo and Rh) atoms into the fcc structure of Pd. Diffraction peaks associated with pure Ir and M (M = Ni, Mo and Rh) atoms or their oxides/hydroxides were not noticed in the XRD patterns. According to the Scherrer formula (Radmilovic *et al*., 1995; Liu *et al*., 2004), the mean crystallite size *d*, predicted from Pd (2 2 0) diffraction peaks, were 3.70, 3.52, 3.37, 3.21, and 3.07 nm for Pd/CC, Pd–Ir/CC, Pd–Ir–Rh/CC, Pd–Ir–Mo/CC, and Pd–Ir–Ni/CC nanoparticles, respectively, which were very close to those attained by TEM.

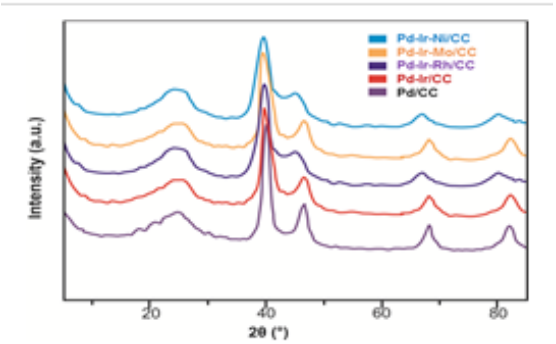

Fig. 1: XRD patterns of Pd/CC, Pd–Ir/CC, Pd–Ir–Ni/CC, Pd–Ir–Mo/CC and Pd–Ir–Rh/CC nanoparticles.

The mean crystallite size and lattice parameters of electrocatalysts attained from the XRD patterns are summarized in Table 2. Pd–Ir/CC and Pd–Ir–M/CC (M = Ni, Mo and Rh) nanoparticles had lesser mean particle sizes than that of Pd/CC nanoparticles. Literally, the reduction of lattice parameter in alloy electrocatalysts showed a continuous improvement in terms of inclusion of Ir and M (M = Ni, Mo and Rh) atoms into the alloy state. Upon comparison between five electrocatalysts, lattice parameters of Pd–Ir–Ni/CC and Pd/CC were found to be the smallest and largest, respectively.

Transmission electron microscopy (TEM)

The size, distribution, and morphology of nanoparticles are known to have considerable effects on the electrocatalyst achievement (Li *et al*., 2012). By considering this, the size of nanoparticles and dispersion of Pd, Pd–Ir, Pd–Ir–Ni, Pd–Ir–Mo, and Pd–Ir–Rh nanoparticles on the sides of CC were measured using TEM as shown in Figure 2. It was observed that the spherical Pd, Pd–Ir, Pd–Ir–Ni, Pd–Ir–Mo, and Pd–Ir–Rh nanoparticles with size ranges from 2–4 nm were homogeneously distributed on the sides of CC. The tiny particle morphology and uniform size dispersion of electrocatalysts were attributed to the faster reduction of metal salts, and an easy formation of metal alloy nanoparticles on CC was promoted by the chemical reduction process assisted by ultrasonication (Lin *et al*., 2012; Hanh *et al*., 2009; Hanh *et al*., 2008). The average particle morphology of the trimetallic nanoparticles (Pd–Ir–Ni/CC, Pd–Ir–Mo/CC and Pd–Ir–Rh/CC) was smaller than that of the monometallic Pd/CC and bimetallic Pd–Ir/CC nanoparticles. For these electrocatalysts, the discrepancy

in the average particle morphology was somewhat identical in both XRD and TEM, which reveals an acceptable particle distribution without formation of big particle accumulations (Table 2).

Table 2: Characterization parameters for the Pd/CC, PD–Ir/CC, Pd–Ir–M/CC (M = Ni, Mo and Rh) nanoparticles.

Nanoparticles		(2 2 0) Diffraction peak position (2θ°)	Lattice parameter (*A*)	Average crystallite size *d* from XRD (nm)	Average Particle size from TEM (nm)
Nominal	Experimental				
Pd_{100}/CC	-	67.82	3.907	3.71	3.91
Pd_{50}–Ir_{50}/CC	Pd_{48}–Ir_{52}/CC	68.21	3.884	3.51	3.29
Pd_{70}–Ir_{20}–Rh_{10}/CC	Pd_{72}–Ir_{19}–Rh_{9}/CC	68.52	3.871	3.38	3.12
Pd_{70}–Ir_{20}–Mo_{10}/CC	Pd_{68}–Ir_{21}– Mo_{11}/CC	68.71	3.860	3.20	3.01
Pd_{70}–Ir_{20}–Ni_{10}/CC	Pd_{71}–Ir_{17}–Ni_{12}/CC	68.93	3.852	3.08	2.72

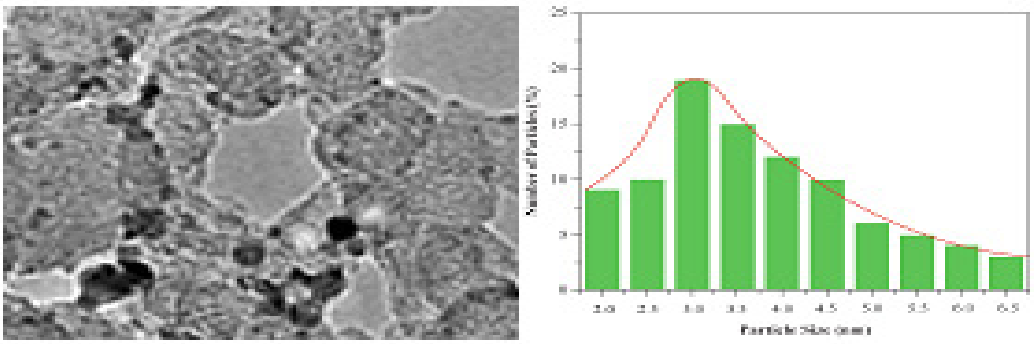

Fig. 2: TEM image and histogram of Pd–Ir–Mo/CC.

Energy dispersive X-ray (EDX) analysis

The metallic composition of Pd/CC, Pd–Ir/CC, Pd–Ir–Ni/CC, Pd–Ir–Mo/CC, and Pd–Ir–Rh/CC was detected using EDX elemental analysis, and results are summarized in Figure 3. The Pd and Ir signals identified in all figures indicate the successful deposition of these atoms on the cellulose-based carbon support.

Chemical characterization

CO stripping

To measure the electrocatalytic activity of synthesized nanoparticles supported on CC for HPOR and the behavior of MLSPBFC, CO_{ads} stripping voltammograms were conducted in 0.5 M H_2SO_4 at room temperature. Figure 4 shows the CO_{ads} stripping voltammograms of Pd–Ir–Ni/CC, Pd–Ir–Mo/CC, Pd–Ir–Rh/CC, Pd–Ir/CC, and Pd/CC nanoparticles at a CO adsorption potential of 0.072 V and a sweep rate of 50 mV s^{-1} in a range of 0.05 V to 0.9 V vs. Ag/AgCl. These environments allowed the withdrawal of adsorbed CO from the initial cycle, followed by the current in the final cycle matched with the standard in case of a pure encouraging electrolyte. In comparison with Pd/CC, a cathodic shift of 150 mV was observed in Pd–Ir–M/CC (M = Ni, Mo and Rh) nanoparticles due to CO oxidation. The positions of peaks in the voltammograms of bimetallic (Pd–Ir/CC) and trimetallic (Pd–Ir–M/CC, M = Ni, Mo and Rh) nanoparticles were identical; but, the peaks of bimetallic nanoparticles were less symmetrical when compared with that of trimetallic nanoparticles. In the voltammograms of tertiary Pd–Ir–M/CC nanoparticles, the higher symmetry of oxidation peaks suggests the occurrence of impressive and powerful electronic interactions between tertiary (Pd–Ir–M, M = Ni, Mo and Rh) nanoparticles and CC.

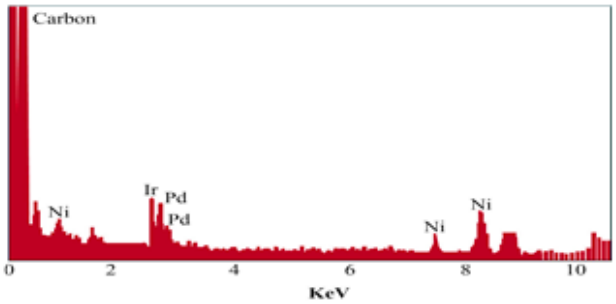

Fig. 3: The EDX spectra of Pd–Ir–Ni/CC.

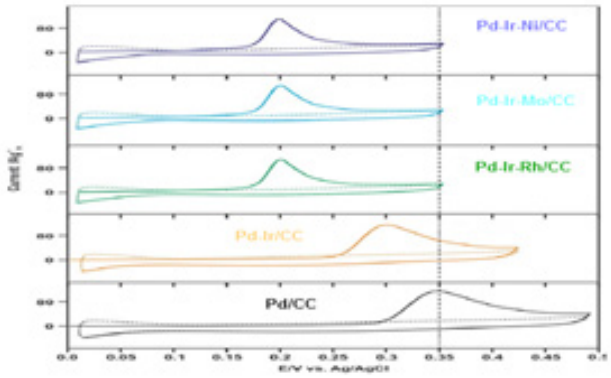

Fig. 4: CO stripping voltammograms of (a) Pd/CC, (b) Pd–Ir/CC, (c) Pd–Ir–Rh/CC, (d) Pd–Ir–Mo/CC and (e) Pd–Ir–Ni/CC nanoparticles in 0.5 M H_2SO_4 at room temperature with a scan rate of 50 mV s^{-1}.

Cyclic voltammetry (CV)

Catalytic activities of the monometallic Pd/CC, bimetallic Pd–Ir/CC, and tri-metallic Pd–Ir–Ni/CC, Pd–Ir–Mo/CC, and Pd–Ir–Rh/CC nanoparticles were studied by CV for the oxidation of hydrogen peroxide. Figure 5 shows CV of nanoparticles reposed on a glassy-carbon electrode without the presence of perborate. The distinct hydrogen adsorption-desorption region (0–0.4 V) was not displayed in voltammograms of catalysts as it was noticed for Pd alloys (Spinace *et al*., 2005). When compared with pure palladium in the double layer region (0.4–0.8 V vs. Ag/AgCl), current for all alloys was higher. The performance of voltammograms was the peculiarity of binary (Pd–Ir/CC) and ternary nanoparticles (Pd–Ir–M/CC, M = Ni, Mo and Rh) containing transition elements (Ribeiro *et al*., 2008; Ribeiro *et al*., 2007). The current values were normalized per gram of Pd by considering the fact that perborate adsorption and dehydrogenation occurred only on palladium sites at room temperature (Zhou *et al*., 2003).

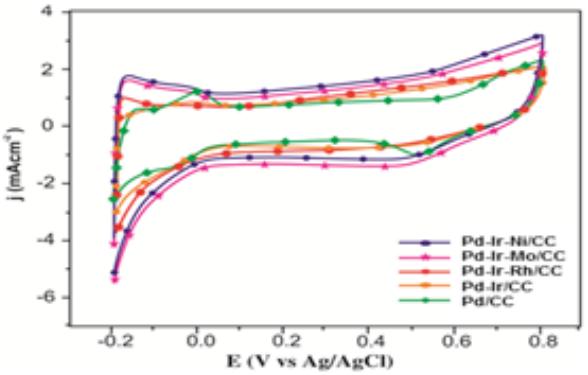

Fig. 5: Cyclic voltammetry of Pd/CC, Pd–Ir/CC and Pd–Ir–M/CC (M = Ni, Mo and Rh), nanoparticles in 0.5 M H_2SO_4 at room temperature with a scan rate of 50 mV s^{-1}.

Electrochemically active surface area (*ECASA*) was estimated by different procedures, such as CO adsorption (*ECASA/CO*), hydrogen adsorption/desorption charge (*ECASA/H*), and roughness of electrodes, to measure the catalytic activity of nanoparticles for hydrogen peroxide oxidation. *ECASA* values of nanoparticles were calculated using the below-mentioned equations (Zhou *et al*., 2003; Bonesi *et al*., 2010; Ribadeneira and Hayos, 2008).

$$S_{ECASA/H}\ (m^2/g) = (Q_H\ (\mu C/cm^2))/(210\ (\mu C/cm^2) * 0.77 * [Pd]) \quad (1)$$

$$S_{ECASA/CO}\ (m^2/g) = (Q_{CO}\ (\mu C/cm^2))/(420\ (\mu C/cm^2) * [Pd]), \quad (2)$$

where Q_H and Q_{CO} are the charges equivalent to desorption of hydrogen and CO on the sides of Pd, respectively; [Pd] (mg cm^{-2}) was the loading of Pd on the sides of electrode; 420 µC/real cm^2 and 210 µC/real cm^2 were the charges required to oxidize a monolayer of CO and hydrogen correspondingly on the surface of Pd; and the coverage of hydrogen monolayer was 0.77 (Biegler *et al*., 1971). Definitely, ternary electrocatalysts (Pd–Ir–M/CC, M = Ni, Mo and Rh) showed close ECASA that were higher than binary electrocatalysts (Pd–Ir/CC) due to the presence of multiple active sites. The unevenness of every electrode was determined by splitting ECASA attained with the probable size. Evaluation of the roughness of electrode and ECASA values are shown in Table 3.

Figure 6 shows CV of hydrogen peroxide oxidation catalyzed by Pd/CC, Pd–Ir/CC, Pd–Ir–Rh/CC, Pd–Ir–Mo/CC, and Pd–Ir–Ni/CC nanoparticles in acidic conditions (0.15 M hydrogen peroxide with 0.5 M H_2SO_4). The voltammograms showed two oxidation peaks: one in the forward scan and the other in the backward scan. During the forward scan, the oxidation peak was observed beyond 1.1 V vs. Ag/AgCl; during the backward scan, the reduction peak was noticed between 0.5 and 0.6 V vs. Ag/AgCl. Thus, CV was conducted below the range of 1.1 and 0.2 V vs. Ag/AgCl. The forward scan was detectable to hydrogen peroxide oxidation, which formed Pd-adsorbed carbonaceous intermediates, including CO and CO_2. The loss of electrochemical activity of the catalyst was due to the adsorbed CO (CO_{ads}) (Huang *et al*., 2005; Liu *et al*., 2004; Hoogers, 2003).

Table 3: Comparison of hydrogen and CO desorption charge, its electrochemical active surface area (ECASA) and electrode roughness.

Catalyst	Q_H/µ	Q_{CO}/µ	Electrode real surface area (cm^2)	*ECASA/H* (m^2/g Fd^{-1})[a]	*SECASA/CO* (m^2/g Fd^{-1})[a]	Roughness
Pd/CC	1374	3570	8.8	85	88	246.4
Pd–Ir/CC	962	2625	625	119	125	175.0
Pd–Ir–Ni/CC	1448	3851	9.16	128	131	248.9
Pd–Ir–Mo/CC	1550	4174	9.93	137	140	269.8
Pd–Ir–Rh/CC	1686	4527	10.7	149	154	292.6

[a] The electrochemical active surface area (*ECASA/H* and *SECASA/CO*) were calculated from Eq. (1) and Eq. (2).

The backward oxidation peak was due to the formation of carbon dioxide through further oxidation of adsorbed carbonaceous species (Hoogers, 2003).

Thus, the current ratio between forward scan peak current (I_F) and backward scan peak current (I_B) displayed the amount of hydrogen peroxide that was oxidized to carbon dioxide with respect to carbon monoxide (Huang *et al*., 2005; Lin *et al*., 2005; Yen *et al*., 2005; Liu *et al*., 2004). A higher I_F/I_B value recommends that electrocatalysts are more effective in reducing the adsorbed CO. The current ratio is an effective way of correlating the long-term electrocatalytic activity of variable catalysts. All CC-supported binary and ternary nanoparticles exhibited a minimum of 60% higher I_F/I_B ratios with respect to that of Pd monometallic nanoparticles (I_F/I_B) 1.32), which was also synthesized by the chemical reduction process assisted by ultrasonication. It was delightful to observe that Pd–Ir/CC bimetallic system showed a higher I_F/I_B ratio next to that of the trimetallic Pd–Ir–Ni, Pd–Ir–Mo, and Pd–Ir–Rh systems. The CV results of synthesized nanoparticles including onset potentials, forward peak current, forward peak potentials, and current ratios (I_F/I_B) of each nanoparticle are summarized in Table 4.

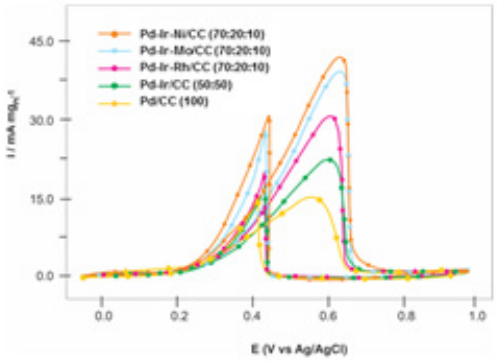

Fig. 6: Cyclic voltammetry of Pd/CC, Pd–Ir/CC and Pd–Ir–M/CC (M = Ni, Mo and Rh) nanoparticles in 0.5 M H_2SO_4 and 0.15 M hydrogen peroxide at room temperature with a scan rate of 50 mV s^{-1}.

The CV results revealed that pure Pd/CC (Figure 6) do not behave as appropriate anodes for the hydrogen peroxide oxidation reaction (HPOR) due to their poisoning by actively adsorbed intermediates, such as CO (Vigier *et al*., 2004). But, the addition of Ir and M (M = Ni, Mo and Rh) improved the catalytic activity of hydrogen peroxide oxidation. The HPOR started at ~0.35 V on Pd/CC electrode, whereas the onset potential on Pd–Ir/CC was recorded at 0.25 V vs. Ag/AgCl, which is in good conformity with the recorded values for Pd–Ir electrocatalyst with a related atomic ratio (Prabhuram *et al*., 2006; Huang *et al*., 2005; Liu *et al*., 2004; Page *et al*., 2000). Furthermore, addition of a third metal M (M = Ni, Mo and Rh) into Pd–Ir/CC considerably decreased the onset potential to ~0.2 V vs. Ag/AgCl (i.e., it was moved to the negative potential by 0.15 V in correlation with Pd/CC) and increased the current density at Pd–Ir–Ni, Pd–Ir–Mo, and Pd–Ir–Rh nanoparticles. The CV results of positive peak potentials and corresponding peak current densities of SPBOR for the synthesized electrocatalysts are summarized in Table 5.

Table 4: CV results of Pd/CC, Pd–Ir/CC, Pd–lr–M/CC (M = Ni, Mo and Rh) nanoparticles at room temperature.

Catalysts	Onset Potential	Forward anodic peak (I_F) (mA cm^{-2})	Backward anodic peak (I_B) (mA cm^{-2})	I_F/I_B ratio
Pd/CC	0.35	20.03	15.26	1.32
Pd–Ir/CC	0.25	37.02	13.15	2.03
Pd–Ir–Rh/CC	0.23	54.07	19.03	2.87
Pd–Ir–Mo/CC	0.21	61.05	20.09	3.06
Pd–Ir–Ni/CC	0.20	74.09	23.96	3.12

When compared with Pd–Ir/CC, the superior activity of Pd–Ir–M/CC observed during the oxidation of hydrogen peroxide can be attributed to the introduction of a third metal (i.e., Ni, Mo and Rh). This effect was confirmed by the hydrogen-spillover phenomena (Wang *et al*., 2006) and modification of Pd electronic states (Liang *et al*., 2006), ended in a sequence of electronic effect and bifunctional method. The catalytic performance of Pd–Ir–Ni was higher than that of the others during the oxidation of hydrogen peroxide, which may result from its higher alloying degree, larger electrochemical surface area, and more improved reaction kinetics.

Table 5: Positive peak potential and Peak current density of Pd/CC, Pd–Ir/CC, Pd–Ir–Rh/CC, Pd–Ir–Mo/CC and Pd–Ir–Ni/CC nanoparticles at room temperature.

Catalyst	Scan rate 50 mV s^{-1}	
	Positive peak potential (V vs. Ag/AgCI)	Peak current density (mA cm^{-2})
Pd/CC	0.75	20.03
Pd–Ir/CC	0.73	37.02
Pd–Ir–Rh/CC	0.72	54.07
Pd–Ir–Mo/CC	0.70	61.05
Pd–Ir–Ni/CC	0.69	74.09

Chronoamperometry (CA)

For practical applications, one of the important requirements is the high persistence of power sources. The longer stability of electrocatalysts towards hydrogen peroxide electro-oxidation was observed in the chronoamperometry measurements by plotting current-time (*i-t*) curves in Figure 7, at a fixed potential of 0.6 V for two hours. In all five CA curves shown in Figure 7, the current gets reduced steadily with time, and it becomes almost stable after some time. The current value might decay because of the uncertainty of electrocatalyst nanoparticles and contamination of the active surface area. Pd–Ir–M/CC (M = Ni, Mo and Rh) nanoparticles showed a higher current at all time points than Pd–Ir/CC nanoparticles and the decomposition ratio of the current density on Pd–Ir–M/CC catalyst was also less than on the Pd–Ir/CC catalyst, which is consistent with the CV results shown in Table 5.

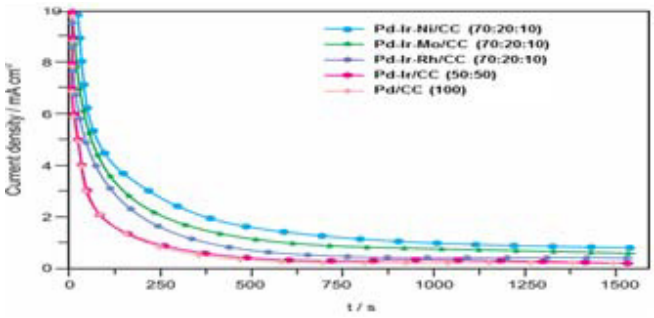

Fig. 7: Chronoamperometry of Pd/CC, Pd–Ir/CC, Pd–Ir–M/CC (M = Ni, Mo and Rh) nanoparticles at room temperature.

Single cell performance

The effects of Pd–Ir–Ni/CC, Pd–Ir–Mo/CC, Pd–Ir–Rh/CC, Pd–Ir/CC, and Pd/CC nanoparticles on hydrogen peroxide electro-oxidation as anode catalysts were calculated in a single MLSPBFC. Figure 8 displays the power density curves and polarization of the MLSPBFC of various catalysts with a loading of 2 mg cm^{-2}. The working environment was 0.15 M hydrogen peroxide and 0.1 M sodium perborate in 0.5 M H_2SO_4 as the anodic and cathodic feed proportionately at room temperature with 300 µL min^{-1} flow rate in each stream. The behavior of the single cell was poor when Pd/CC was used as an anode catalyst. The OCP was 0.49 V, which was significantly lesser than the reversible OCP (1.145 V). This is primarily associated with the lowered electrocatalytic activity and CO poisoning towards hydrogen peroxide oxidation. Table

6 summarizes the results of MLSPBFC adapting to various electrocatalysts.

It was noted that the behavior of Pd–Ir–Ni/CC was better than that of the other corresponding ternary, binary, and monometallic electrocatalysts during the distribution of current to the single cell structural area. The power taken from a single cell was relatively same for all electrocatalysts, except for the monometallic Pd/CC, in the low current flow region. But, Pd–Ir–Ni/CC initiated drawing more current when compared to other electrocatalysts. The OCP for bimetallic Pd–Ir/CC was lesser than ternary Pd–Ir–M/CC (M = Ni, Mo and Rh) nanoparticles. Moreover, a speedy initial fall in the cell voltage was observed for all electrocatalysts as a result of slow initial hydrogen peroxide electro-oxidation reaction at the sides of the electrode. After an initial reduction, the change in slope of the polarization curve for Pd–Ir–Ni/CC got reduced and more current was produced. This is associated with more powerful catalytic ability of Pd–Ir–Ni/CC when the hydrogen peroxide electro-oxidation reaction is started. According to the principle of peak power density taken from a single cell, Pd–Ir–Ni/CC was the best anode catalyst with a higher peak power density than other tested catalysts. The output results were identical as like CV and CA measurements. The increase in behavior was due to the introduction of the third metal M into Pd–Ir/CC catalyst for hydrogen peroxide oxidation. Such effect could be examined in three prospects: the electronic effect, the hydrogen spillover effect, and the bifunctional mechanism. Based on the results, it is clear that the electron density of the third metal M (M = Ni, Mo and Rh) was getting transferred to Pd. The electrocatalytic sites would enlarge as a result of the adsorption of CO_{ads} on Pd surface was decreased due to the decrease in Pd–CO binding energy. Furthermore, the bifunctional mechanism had been investigated in earlier studies as shown below (Arun *et al.*, 2015).

$$MO_x + H_2O \rightarrow MO_x\text{–}OH_{ads} + H^+ + e^-$$

$$Pd\text{–}CO_{ads} + MO_x\text{–}OH_{ads} \rightarrow Pd + MO_x + CO_2 + H^+ + e^-.$$

Taken together, it is evident that MO_x improves the activation of water to generate the species of OH_{ads}, which could have ended up with CO oxidation; therefore, increase the activity of Pd–Ir–M/CC (M = Ni, Mo and Rh) nanoparticles for HPOR.

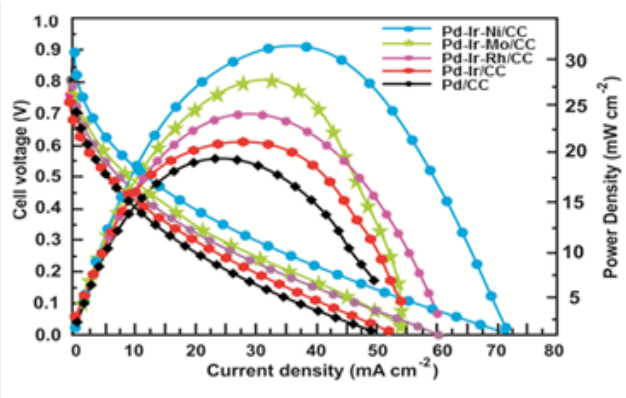

Fig. 8: Polarization and power denity curves of Pd/CC, Pd–Ir/CC and Pd–Ir–M/CC (M = Ni, Mo and Rh) nanoparticles.

Table 6: Performance of single fuel cell test using Pd/CC, Pd–Ir/CC and Pd–Ir–M/CC (M = Ni, Mo and Rh) nanoparticles.

Anode Catalysts	Open circuit voltage (V)	Maximum power density (mW cm^{-2})	Maximum current density (mA cm^{-2})
Pd/CC	0.69	22.14	145
Pd–Ir/CC	0.75	28.01	205
Pd–Ir–Rh/CC	0.82	30.34	232
Pd–Ir–Mo/CC	0.86	31.14	246
Pd–Ir–Ni/CC	0.92	32..31	257

Moreover, in biological science, carbon-based nanomaterials have been utilized as excellent platforms for facilitating biochemical reactions and processes, such as sensitive recognition of antibodies, sequencing of nucleic acids, bioseparation, and biocatalysis. Single-walled nanotubes exhibit much stronger antibacterial activity than multi-walled nanotubes, suggesting that CNT size (diameter) plays an important role in the inactivation of bacterial cells. Literature survey reveals that virtually all carbon nanomaterials can able to show antibacterial properties.

CONCLUSION

In this study, Pd, Pd–Ir, and Pd–Ir–M (M = Ni, Mo and Rh) nanoparticles supported on cellulose-based carbon were successfully synthesized by the chemical reduction process. Ternary nanoparticles (Pd–Ir–M/CC, M = Ni, Mo and Rh) showed high electrochemically active surface area and improved electrocatalytic activity than that of binary nanoparticles (Pd–Ir/CC) for hydrogen peroxide oxidation. This study provides a simple way to prepare such electrocatalysts while enhancing the electrochemical performance. The effect of operating conditions on the performance on an MLSPBFC with Pd/CC, Pd–Ir/CC, Pd–Ir–Ni/CC, Pd–Ir–Mo/CC, and Pd–Ir–Rh/CC as anode catalysts was investigated. The performance on an MLSPBFC using Pd–Ir–Ni/CC as the anode catalyst was better than that of other catalysts synthesized by the same method, which could be attributed to the electronic effect, bifunctional mechanism, and hydrogen spill over. These results indicate that CC could be good candidates to use as supporting materials in high loading metal catalysts in fuel cells. The durability of the MLSPBFC was examined under acidic media in a period of about 2 hours. The MLSPBFC maintained a relatively stable performance with a little decay of cell voltage over the test period. The fluctuation in the cell voltage was due to the addition of a new fuel solution, restarting the experiments or a small variation in cell temperature. The result of the durability test showed that the MLSPBFC in our research has good stability at room temperature, which is able to satisfy the necessary conditions as portable power sources.

ACKNOWLEDGMENT

The financial support for this research from University Grants Commission (UGC), New Delhi, India through a Major Research Project 42–325/2013 (SR) is gratefully acknowledged.

CONFLICT OF INTEREST

The authors declare that they have no conflict of interest.

REFERENCES

Ahn SH, Choi I, Kwon OJ, Kim JJ. One-step co-electrodeposition of Pt–Ru electrocatalysts on carbon paper for direct methanol fuel cell.

Chem Eng, 2012; 181-182:276-280.

Arun A, Gowdhamamoorthi M, Ponmani K, Kiruthika S, Muthukumaran B. Electrochemical characterization of Pt–Ru–Ni/C anode electrocatalyst for methanol electrooxidation in membraneless fuel cells. RSC Adv, 2015; 5(61):49643-49650.

Basnayake R, Li Z, Katar S, Zhou W, Rivera H, Smotkin ES, Casadonte DJ, Korzeniewski C. PtRu nanoparticle electrocatalyst with bulk alloy properties prepared through a sonochemical method. Langmuir, 2006; 22(25):10446-10450.

Bennett B, Koraishy BM, Meyers JP. Mode$_{lin}$g and optimization of the DMFC system: Relating materials properties to system size and performance. J Power Source, 2012; 218:268-279.

Biegler T, Rand DAJ, Woods R. Limiting oxygen coverage on platinized platinum; Relevance to determination of real platinum area by hydrogen adsorption. J Electroanal. Chem, 1971; 29(2):269-277.

Bonesi AR, Moreno MS, Triaca WE, Castro Luna AM. Modified catalytic materials for ethanol oxidation. Int. J Hydrogen Energy, 2010; 35(11):5999-6004.

Che G, Lakshmi BB, Martin CR, Fisher ER. Metal-Nanocluster-Filled Carbon Nanotubes: Catalytic Properties and Possible Applications in Electrochemical Energy Storage and Production. Langmuir, 1999; 15(3):750-758.

Collins PG, Zettl A, Bando H, Thess A, Smalley RE. Nanotube Nanodevice. Science, 1997; 278(5335):100-102.

Correa-Duarte MA, Liz-Marzan LM. Carbon nanotubes as templates for one-dimensional nanoparticle assemblies. J Mater Chem, 2006; 16(1):22-25.

Cui HF, Ye JS, Liu X, Zhang WD, Sheu FS. Pt–Pb alloy nanoparticle/carbon nanotube nanocomposite: a strong electrocatalyst for glucose oxidation. Nanotechnology, 2006; 17(9):2334-2339.

Dillon AC, Jones KM, Bekkedahl TA, Kiang CH, Bethune DS, Heben MJ. Storage of hydrogen in single-walled carbon nanotubes. Nature, 1997; 386(6623):377-379.

Escudero-Cid R, Hernandez-Fernandez P, Perez-Flores JC, Rojas S, Garcia-Rodriguez S, Fatas E, Ocon P. Analysis of performance losses of direct methanol fuel cell with methanol tolerant PtCoRu/C cathode electrode. Int J Hydrogen Energy, 2012; 37(8):7119-7130.

Gavillon R, Budtova T. Aerocellulose: New highly porous cellulose prepared from cellulose – NaOH aqueous solutions. Biomacromolecules, 2008; 9:269-277.

Georgakilas V, Gournis D, Tzitzios V, Pasquato L, Guldi DM, Prato M. Decorating carbon nanotubes with metal or semiconductor nanoparticles. J Mater Chem, 2007; 17(26):2679-2694.

Grag A, Sinnott SB. Effect of chemical functionalization on the mechanical properties of carbon nanotubes. Chem Phys Lett, 1998; 295(4):273-278.

Guillen-Villafuerte O, Guil-Lopez R, Nieto E, Garcia G, Rodriguez JL, Pastor E, Fierro JLG. Electrocatalytic performance of different Mo-phases obtained during the preparation of innovative Pt-MoC catalysts for DMFC anode. Int J Hydrogen Energy, 2012; 37(8):7171-7179.

Hanh HD, Dong NT, Okitsu K, Nishimura R, Maeda Y. Biodiesel production through transesterification of triolein with various alcohols in an ultrasonic field. Renewable Energy, 2009; 34(3):766-768.

Hanh HD, Dong NT, Okitsu K, Starvarache C, Okitsu K, Maeda Y, Nishimura R. Methanolysis of triolein by low frequency ultrasonic irradiation. Energy Convers Manage, 2008; 49(2):276-280.

He D, Yang L, Kuang S, Cai Q. Fabrication and catalytic properties of Pt and Ru decorated TiO_2\CNTs catalyst for methanol electrooxidation. Electrochem Commun, 2007; 9(10):2467-2472.

Hoogers G. Fuel Cell Technology Handbook: The fueling problem: Fuel cell systems. Boca Raton: CRC Press, 2002; 5-1:5-40

Huang T, Liu J, Li R, Cai W, Yu A. A novel route for preparation of PtRuMe (Me = Fe, Co, Ni) and their catalytic performance for methanol electrooxidation. Electrochem Commun, 2009; 11(3):643-646.

Huang J, Liu Z, He C, Gan LM. Synthesis of PtRu Nanoparticles from the Hydrosilylation Reaction and Application as Catalyst for Direct Methanol Fuel Cell. J Phys. Chem. B, 2005; 109(35):16644-16649.

Jeon MK, Lee KR, Daimon H, Nakahara A, Woo SI. $Pt_{45}Ru_{45}M_{10}$/C (M = Fe, Co, and Ni) catalysts for methanol electro-oxidation. Catal Today, 2008; 132(1-4):123-126.

Jin C, Chen Z. Electrocatalytic oxidation of glucose on gold–platinum nanocomposite electrodes and platinum-modified gold electrodes. Synthetic Metals, 2007; 157(13-15):592-596.

Kakati N, Lee SH, Maiti J, Yoon YS. Ru decorated Pt nanoparticles by a modified polyol process for enhanced catalytic activity for methanol oxidation. Surf Sci, 2012; 606(21-22):1633-1637.

Kang S, Lim S, Peck DH, Kim SK, Jung DH, Hong SH, Jung HG, Shul Y. Stability and durability of PtRu catalysts supported on carbon nanofibers for direct methanol fuel cells. Int J Hydrogen Energy, 2012; 37(5):4685-4693.

Lamy C, Lima A, LeRhun V, Delime F, Coutanceau C, Leger JM. Recent advances in the development of direct alcohol fuel cells (DAFC). J Power Sources, 2002; 105(2):283-296.

Li QX, Xu Q, Zhou X, Li J. Preparation and Electrochemical Research of Anode Catalyst PtRuNi/C for Direct Methanol Fuel Cell. J Biobased Bio, 2013; 7(4):525-528.

Li B, Higgins DC, Zhu S, Li H, Wang H, Ma J, Chen Z. Highly active Pt–Ru nanowire network catalysts for the methanol oxidation reaction. Catal Commun, 2012; 18:51-54.

Liang Y, Zhang H, Tian Z, Zhu X, Wang X, Yi B. Synthesis and Structure−Activity Relationship Exploration of Carbon-Supported PtRuNi Nanocomposite as a CO-Tolerant Electrocatalyst for Proton Exchange Membrane Fuel Cells. J Phys. Chem. B, 2006; 110(15):7828-7834.

Lin CC, Hsiao MC, Liao PH. Ultrasonic-assisted production of biodiesel from waste frying oil using a two-step catalyzing process. J Sustain Bioenergy Syst, 2012; 2(4):117-121.

Lin Y, Cui X, Yen C, Wai CM. Platinum/Carbon Nanotube Nanocomposite Synthesized in Supercritical Fluid as Electrocatalysts for Low-Temperature Fuel Cells. J Phys. Chem. B, 2005; 109(30):14410-14415.

Liu F, Lee JY, Zhou W. Multi-Segment Pt–RuNi Nanorods for Methanol Electro-Oxidation at Room Temperature. J Electrochem Soc, 2006; 153(11):A2133-A2138.

Liu H, Song C, Zhang L, Zhang J, Wang H, Wilkinson DP. A review of anode catalysis in the direct methanol fuel cell. J Power Sources, 2006; 155(2):95-110.

Liu Z, Ling XY, Su X, Lee JY. Carbon-Supported Pt and PtRu Nanoparticles as Catalysts for a Direct Methanol Fuel Cell. J Phys. Chem. B, 2004; 108(24):8234-8240.

Nethravathi C, Anumol EA, Rajamathi M, Ravishankar N. Highly dispersed ultrafine Pt and PtRu nanoparticles on graphene: formation mechanism and electrocatalytic activity. Nanoscale, 2011; 3(2):569-571.

Page T, Johnson R, Hormes J, Noding S, Rambabu B. A study of methanol electro-oxidation reactions in carbon membrane electrodes and structural properties of Pt alloy electro-catalysts by EXAFS. J Electroanal. Chem, 2000; 485(1):34-41.

Park SH, Jung HM, Um S, Song YW, Kim HS. Rapid synthesis of Pt-based alloy/carbon nanotube catalysts for a direct methanol fuel cell using flash light irradiation. Int J Hydrogen Energy, 2012; 37(17):12597-12604.

Prabhuram J, Zhao TS, Tang ZK, Chen R, Liang ZX. Multiwalled Carbon Nanotube Supported PtRu for the Anode of Direct Methanol Fuel Cells. J Phys. Chem. B, 2006; 110(11):5245-5252.

Radmilovic V, Gasteiger HA, Ross Jr. PN. Structure and chemical composition of a supported Pt-Ru electrocatalyst for methanol oxidation. J. Catal, 1995; 154(1):98-106.

Ribadeneira E, Hayos BA. Evaluation of Pt–Ru–Ni and Pt–Sn–Ni catalysts as anodes in direct ethanol fuel cells. J Power Sources, 2008; 180(1):238-242.

Ribeiro LS, Delgado JJ, Orfao JJM, Pereira MFR. Carbon supported Ru-Ni bimetallic catalysts for the enhanced one-pot conversion of cellulose to sorbitol. Applied Catalysis B: Environmental, 2017; 217:265-274.

Ribeiro J, dos Anjos DM, Leger J-M, Hahn F, Olivi P, de Andrade AR, Tremiliosi-Filho G, Kokoh KB. Effect of W on PtSn/C catalysts for ethanol electrooxidation. J Appld. Electrochem, 2008; 38(5):653-662.

Ribeiro J, dos Anjos DM, Kokoh KB, Coutanceau C, Leger J-M, Olivi P, de Andrade AR, Tremiliosi-Filho G. Carbon-supported ternary PtSnIr catalysts for direct ethanol fuel cell. Electrochim Acta, 2007; 52(24):6997-7006.

Rodriguez-Nieto FJ, Morante-catacora TY, Cabrera CR. Sequential and simultaneous electrodeposition of Pt–Ru electrocatalysts on a HOPG substrate and the electro-oxidation of methanol in aqueous sulfuric acid. J Electroanal Chem, 2004; 571(1):15-26.

Ryu J, Kim K, Kim HS, Hahn HT, Lashmore D. Intense pulsed light induced platinum-gold alloy formation on carbon nanotubes for non-enzymatic glucose detection. Biosens Bioelectron, 2010; 26(2):602-607.

Shahrokhian S, Rastgar S. Electrodeposition of Pt–Ru nanoparticles on multi-walled carbon nanotubes: Application in sensitive voltammetric determination of methyldopa. Electrochim Acta, 2011; 58:125-133.

Spinace EV, Linardi M, Neto AO. Co-catalytic effect of nickel in the electro-oxidation of ethanol on binary Pt–Sn electrocatalysts. Electrochemistry Communications, 2005; 7(4):365-369.

Tusi MM, Brandalise M, Polanco NSO, Correa OV, Silva AC, Villalba JC, Anaissi FJ, Neto AO, Spinace EV. Ni/Carbon Hybrid Prepared by Hydrothermal Carbonization and Thermal Treatment as Support for PtRu Nanoparticles for Direct Methanol Fuel Cell. J Mater Sci Technol, 2013; 29(8):747-751.

Umeda M, Ueda M, Shironita S. Novel O_2-enhancing Methanol Oxidation at Pt-Ru-C Sputtered Electrode: Direct Methanol Fuel Cell Power Generation Performance. Energy Procedia, 2012; 28:102-112.

Vigier F, Coutanceau C, Hahn F, Belgsir EM, Lamy C. On the mechanism of ethanol electro-oxidation on Pt and PtSn catalysts: electrochemical and *in situ* IR reflectance spectroscopy studies. J Electroanal Chem, 2004; 563(1):81-89.

Wang ZB, Yin GP, Shi PF, Sun YC. Novel Pt–Ru–Ni/C Catalysts for Methanol Electro-oxidation in Acid Medium. Electrochem. Solid State Lett, 2006; 9(1):A13-A15.

Wang ZB, Zuo PJ, Wang GJ, Du CY, Yin GP. Effect of Ni on PtRu/C Catalyst Performance for Ethanol Electrooxidation in Acidic Medium. J Phys Chem C, 2008; 112(16):6582-6587.

Wang W, Wang R, Wang H, Ji S, Key J, Li X, Lei Z. An advantageous method for methanol oxidation: Design and fabrication of a nanoporous PtRuNi trimetallic electrocatalyst. J Power Sources, 2011; 196(22):9346-9351.

Wei ZD, Li LL, Luo YH, Yan C, Sun CX, Yin GZ, Shen PK. Electrooxidation of Methanol on upd-Ru and upd-Sn Modified Pt Electrodes. J Phys Chem B, 2006; 110(51):26055-26061.

Xiong L, Manthiram A. Effect of Atomic Ordering on the Catalytic Activity of Carbon Supported PtM (M = Fe, Co, Ni, and Cu) Alloys for Oxygen Reduction in PEMFCs. J Electrochem Soc, 2005; 152(4):A697-A703.

Yang DS, Sim KS, Kwen HD, Choi SH. One-step preparation of Pt–M@FP-MWNT catalysts (M = Ru, Ni, Co, Sn, and Au) by γ-ray irradiation and their catalytic efficiency for CO and MeOH. J Ind Eng Chem, 2012; 18(1):538-545.

Yen CH, Cui X, Pan HB, Wang S, Lin Y, Wai CM. Deposition of Platinum Nanoparticles on Carbon Nanotubes by Supercritical Fluid Method. J Nanosci. Nanotechnol, 2005; 5(11):1852-1857.

Zhang ZQ, Liu B, Chen YL, Jiang H, Hwang KC, Huang Y. Mechanical properties of functionalized carbon nanotubes. Nanotech, 2008; 19(39):395702.

Zhao X, Li W, Fu Y, Manthiram A. Influence of ionomer content on the proton conduction and oxygen transport in the carbon-supported catalyst layers in DMFC. Int J Hydrogen Energy, 2012; 37(12):9845-9852.

Zheng W, Suominen A, Tuominen A. Discussion on the Challenges of DMFC Catalyst Loading Process for Mass Production. Energy Procedia, 2012; 28:78-87.

Zhao Y, E Y, Fan L, Qiu Y, Yang S. A new route for the electrodeposition of platinum-nickel alloy nanoparticles on multi-walled carbon nanotubes. Electrochim Acta, 2007; 52(19):5873-5878.

Zhou Z, Wang S, Zhou W, Wang G, Jiang L, Li W, Song S, Liu J, Sun G, Xin Q. Novel synthesis of highly active Pt/C cathode electrocatalyst for direct methanol fuel cell. Chem Commu, 2003; (3):394-395.

How to cite this article:
Vijayaramalingam K, Karthikeyan A, Selvarani V, Kiruthika S, Muthukumaran B. Enhanced Electrocatalytic Activity of Pd–Ir–Ni, Pd–Ir–Mo and Pd–Ir–Rh Nanoparticles Supported on Cellulose-based Carbon (CC) for Membraneless Sodium Perborate Fuel Cells (MLSPBFCs). J App Pharm Sci, 2018; 8(08): 129-137.